

## Inelastic polarized and unpolarized neutron scattering measurements on $\text{UBe}_{13}$

A. I. Goldman, S. M. Shapiro, and G. Shirane

*Department of Physics, Brookhaven National Laboratory, Upton, New York 11973*

J. L. Smith and Z. Fisk

*Materials Science and Technology Division, Los Alamos National Laboratory,*

*University of California, Los Alamos, New Mexico 87545*

(Received 25 June 1985)

We present the results of polarized and unpolarized inelastic neutron scattering measurements of the heavy-fermion superconductor  $\text{UBe}_{13}$  at 10 K. At this temperature, the energy spectrum of the magnetic scattering is characterized by a broad quasielastic Lorentzian line shape modified by the Bose occupation factor, with a width of  $13 \pm 2$  meV (half-width at half maximum). No evidence of a narrow (few meV)  $f$ -level resonance predicted by the electronic specific-heat coefficient is observed. The energy-integrated magnetic scattering yields a susceptibility which is consistent with bulk measurements, indicating that any additional response must have a small spectral weight.

### I. INTRODUCTION

The discovery of superconductivity in heavy-fermion systems such as  $\text{CeCu}_2\text{Si}_2$ ,  $\text{UBe}_{13}$ , and  $\text{UPt}_3$  has stimulated new investigations of both the normal and superconducting state of these materials.<sup>1</sup>  $\text{UBe}_{13}$  is one of the first established heavy-fermion superconductors.<sup>2</sup> In the normal state, at low temperature, the electronic specific-heat coefficient ( $\gamma$ ) of this material is  $1.1$  J/mole $\text{K}^2$ , yielding an effective mass for the uranium  $5f$  electrons of several hundred times the free-electron value. The large specific-heat jump of approximately  $1$  J/mole K at the superconducting transition temperature ( $T_c \approx 0.9$  K) indicates that these same  $f$  electrons are responsible for the superconductivity. The magnetic susceptibility of  $\text{UBe}_{13}$  near room temperature exhibits Curie-Weiss behavior. However, below  $\sim 150$  K the susceptibility deviates from this simple dependence and approaches a large finite value at low temperature. Both the large values for the specific heat and susceptibility at low temperature have led to the description of  $\text{UBe}_{13}$  as a Fermi-liquid system.<sup>2</sup>

Inelastic neutron scattering measurements, which couple directly to the response of the  $f$ -electrons, are a powerful probe of spin fluctuations. In the heavy-fermion systems, the large value of  $\gamma$  suggests a narrow peak in the density of states for the  $f$  electrons at the Fermi energy. Previous neutron scattering studies of  $\text{CeCu}_2\text{Si}_2$  (Ref. 3) ( $\gamma = 1.1$  J/mole $\text{K}^2$ ) have indeed observed a narrow quasielastic feature in the magnetic spectrum with a half-width,  $\Gamma$ , of about  $1$  meV at  $T = 10$  K. Recent polarized neutron scattering measurements on  $\text{UPt}_3$  (Ref. 4) ( $\gamma = 0.45$  J/mole $\text{K}^2$ ) have yielded a quasielastic line in the magnetic cross section with  $\Gamma = 10 \pm 2$  meV at  $T = 1.3$  K. Here we report inelastic polarized and unpolarized neutron scattering measurements on  $\text{UBe}_{13}$  at  $10$  K. In this system we have observed a quasielastic response which is significantly broader ( $\Gamma = 13 \pm 2$  meV) than that expected on the basis of specific-heat measurements.

### II. EXPERIMENTAL PROCEDURE

Both  $\text{UBe}_{13}$  and  $\text{ThBe}_{13}$  crystallize in the cubic  $\text{NaZn}_{13}$ -type structure [space group  $O_h^6$  ( $Fm\bar{3}c$ )]. There are eight formula units per unit cell, with  $8M$  (U,Th) in the positions 8(a):  $\pm \frac{1}{4}, \frac{1}{4}, \frac{1}{4}$ ;  $8\text{Be(I)}$  in 8(b):  $0, 0, 0, \frac{1}{2}, \frac{1}{2}, \frac{1}{2}$ ; and  $96\text{Be(II)}$  in the general positions 96(i):  $0, y, z$  etc.<sup>5</sup> Recent neutron diffraction measurements<sup>6</sup> of both  $\text{UBe}_{13}$  and  $\text{ThBe}_{13}$  determined the lattice constants and  $y, z$  positional parameters summarized in Table I at  $10$  K.

Specimens of  $\text{UBe}_{13}$  and  $\text{ThBe}_{13}$  were prepared using a method described elsewhere,<sup>2</sup> powdered, and sieved through a screen with  $420\text{-}\mu\text{m}$  openings. Approximately  $24$  g of polycrystalline  $\text{UBe}_{13}$  ( $20$  g of  $\text{ThBe}_{13}$ ) were loaded into a  $2.5$  cm high and  $2.5$  cm in diameter cylindrical aluminum sample holder. Thin circular sheets of cadmium, separated  $6\text{-mm}$  layers of powder to reduce multiple scattering. The sample holder was sealed in an Al outer can filled with helium to ensure good thermal transfer and attached to the cold finger of a Displex refrigerator.

#### A. Unpolarized-beam measurements

Unpolarized-neutron-beam measurements of both  $\text{UBe}_{13}$  and  $\text{ThBe}_{13}$  were made on a triple-axis spectrometer using a pyrolytic graphite (PG) (002) monochromator and analyzer, and a PG filter before the monochromator to reduce  $\lambda/2$  contamination of the incident beam. Mea-

TABLE I. Structural parameters of  $\text{UBe}_{13}$  and  $\text{ThBe}_{13}$  at  $10$  K.

System	$a_0$ (Å)	$v$	$z$
$\text{UBe}_{13}$	10.248 87(2)	0.1763(1)	0.1150(1)
$\text{ThBe}_{13}$	10.410 05(3)	0.1745(1)	0.1129(1)

TABLE II. Energy resolution for spectrometer configurations.

$E_I$ (meV)	$E_F$ (meV)	Collimation	$\Delta E$ (meV)
Unpolarized beam			
(a) 5.0 <sup>a</sup>	5.0	40'-40'-40'-40'	0.15
(b) 30.5 <sup>a</sup>	30.5	40'-20'-40'-40'	2.0
(c) 41.0	41.0 <sup>a</sup>	40'-20'-40'-40'	3.7
(d) 41.0 <sup>a</sup>	41.0	40'-40'-40'-40'	4.3
Polarized beam			
(e) 42.0	42.0 <sup>a</sup>	40'-80'-80'-80'	8
(f) 42.0	42.0 <sup>a</sup>	40'-80'-80'-open	9

<sup>a</sup>Denotes fixed during scan.

measurements were performed at several fixed incident or final energies and collimations. Table II summarizes the energy resolution which results from these instrumental configurations.

The inelastic unpolarized neutron scattering spectrum of  $\text{UBe}_{13}$  consists of both magnetic and phonon contributions. This is illustrated nicely in Fig. 1, which shows the energy-loss spectra measured at constant  $Q=2.0$  and  $6.0 \text{ \AA}^{-1}$ . For neutron energy loss between 0 and 13 meV, the scattering at the higher  $Q$  is significantly smaller than that at small  $Q$ , as is expected for the electronic form-factor  $Q$  dependence of magnetic scattering. The feature at 13 meV, however, is significantly enhanced at the larger  $Q$ , implying that it is due to phonons.

In order to isolate the paramagnetic scattering from

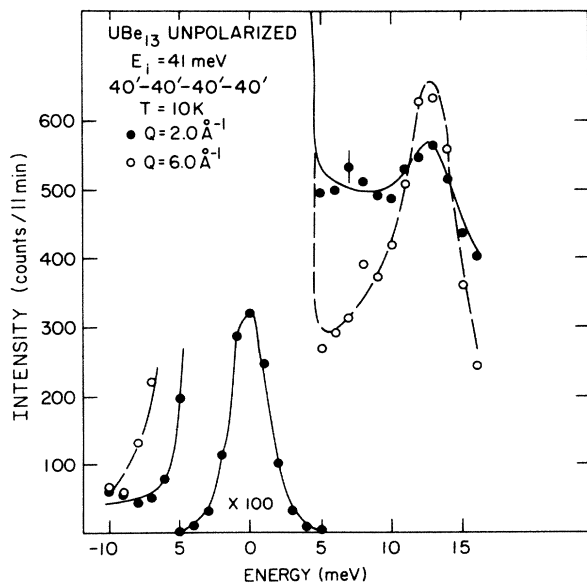


FIG. 1. Inelastic unpolarized neutron scattering spectra of  $\text{UBe}_{13}$  at 10 K for  $Q=2.0$  and  $6.0 \text{ \AA}^{-1}$ .

polycrystalline  $\text{UBe}_{13}$  in the unpolarized-neutron measurements, the phonon contribution to the inelastic spectrum must be subtracted.<sup>7</sup> Fortunately, as noted above, the nonmagnetic compound  $\text{ThBe}_{13}$  has the same structure as  $\text{UBe}_{13}$ , while the scattering lengths of U and Th differ by very little. Therefore, the phonon density of states in  $\text{ThBe}_{13}$  should be similar to that in  $\text{UBe}_{13}$ , and this can be tested. Bragg powder peaks from  $\text{UBe}_{13}$  and  $\text{ThBe}_{13}$  were used to calculate the difference in effective sample volume for these two samples, and using the known scattering lengths for U and Th, a normalization constant ( $N$ ) was calculated to account for these differences. The magnetic scattering contribution for  $\text{UBe}_{13}$  is then calculated from

$$I_{\text{mag}}(\text{UBe}_{13}) = I(\text{UBe}_{13}) - NI(\text{ThBe}_{13}). \quad (1)$$

### B. Polarized-beam measurements

A second, more direct means of eliminating the nuclear background and isolating the magnetic scattering from  $\text{UBe}_{13}$ , is to perform inelastic polarized neutron scattering measurements.<sup>8</sup> The disadvantage of this method is much lower signal rates, which requires some compromise in energy resolution, and longer counting times.

These measurements were made on a modified triple-axis spectrometer using vertically magnetized Heusler (111) transmission crystals at the monochromator and analyzer positions, magnetic guide fields to maintain the polarization of the neutrons, and a flipping coil between the sample and analyzer. A small magnetic field at the sample is used to orient the neutron polarization either along the scattering vector (HF) or perpendicular to the scattering plane (VF) in this region. The inelastic spectra were measured at constant  $Q$  with a fixed final energy of 42 meV and collimations of 40'-80'-80'-open, providing an energy resolution of about 9 meV (full width at half maximum) at  $\omega=0$ . The overall flipping ratio of the instrument, which measures the sensitivity of detection of spin-flip (magnetic) to non-spin-flip (nuclear) events, was 15 for both HF and VF.

In Table III we show the four possible measurements of spin-flip (flipper on) and non-spin-flip (flipper off) scattering with HF and VF for an isotropic paramagnet.<sup>9</sup> In the flipper on channel, the difference HF-VF yields  $\frac{1}{2}$  of the magnetic cross section measured in the unpolarized neutron scattering experiment, and the contributions from background and nuclear-spin incoherent scattering cancel.

TABLE III. Polarized neutron scattering measurements on powders.  $M = (S_{xx} + S_{yy} + S_{zz})$ ;  $\mathcal{S}_{\text{NSI}}$  is the nuclear spin incoherent contribution;  $N$  is the nuclear contribution;  $B, B' \equiv$  background;  $S^z$  is taken along  $Q$ .

	Flipper on	Flipper off
HF	$S_{xx} + S_{yy} + \frac{2}{3}\mathcal{S}_{\text{NSI}} + B$	$N + \frac{1}{3}\mathcal{S}_{\text{NSI}} + B'$
VF	$S_{xx} + \frac{2}{3}\mathcal{S}_{\text{NSI}} + B$	$S_{yy} + N + \frac{1}{3}\mathcal{S}_{\text{NSI}} + B'$

### III. RESULTS AND ANALYSIS

Figure 2(a) shows the inelastic unpolarized measurements of  $\text{UBe}_{13}$  and  $\text{ThBe}_{13}$  at 10 K for  $Q=2.0 \text{ \AA}^{-1}$ . Here, the  $\text{ThBe}_{13}$  data has been multiplied by a normalization constant ( $N=1.1$ ) as described in Sec. II. The  $\text{ThBe}_{13}$  spectrum exhibits a sharp feature at  $\omega=13 \text{ meV}$  which, as we postulated in the discussion of Fig. 1, corresponds to a peak in the phonon density of states. A similar, but broadened peak is observed in the  $\text{UBe}_{13}$  spectrum. The increase in scattering at higher energies, evident in both spectra, is the start of a band of phonons associated with the vibrations of the Be atoms.<sup>7</sup> The difference between the two spectra, as well as the apparent broadening of the peak at  $\omega=13 \text{ meV}$ , is due to the magnetic scattering contribution to  $\text{UBe}_{13}$ . To test this, we have performed a  $Q$ -scan at constant energy transfer ( $\omega=12 \text{ meV}$ ) for both samples. Figure 3 shows that the difference between the spectra,  $I(\text{UBe}_{13}) - 1.27I(\text{ThBe}_{13})$ ,<sup>10</sup> decreases with increasing  $Q$ , consistent with the  $\text{U}^{2+}$   $5f$ -electron form factor<sup>11</sup> shown as the solid line in Fig. 3. It was not possible from these measurements to determine whether the  $Q$  dependence was closer to the  $\text{U}^{2+}$  or  $\text{U}^{3+}$  form factor since they may be distinguished only at large  $Q$ , where the signal is weak. However, the fact that the subtracted spectrum follows the uranium- $5f$  form factor

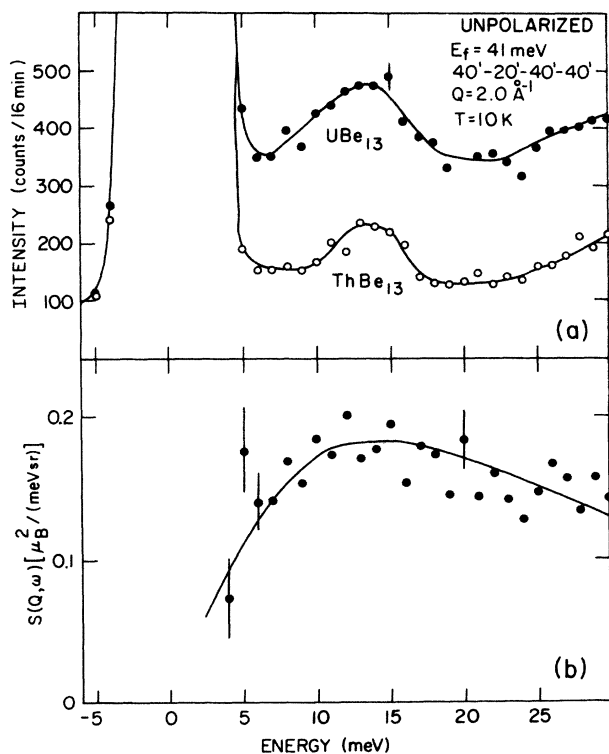


FIG. 2. (a) Inelastic unpolarized spectra of  $\text{UBe}_{13}$  and  $\text{ThBe}_{13}$  at 10 K. The latter has been scaled by  $N=1.1$  as described in the text. (b) The difference spectrum,  $I(\text{UBe}_{13}) - 1.1 \times I(\text{ThBe}_{13})$  in absolute units for the magnetic cross section. The solid line is a fit to the data using a quasielastic Lorentzian modified by the occupation factor.

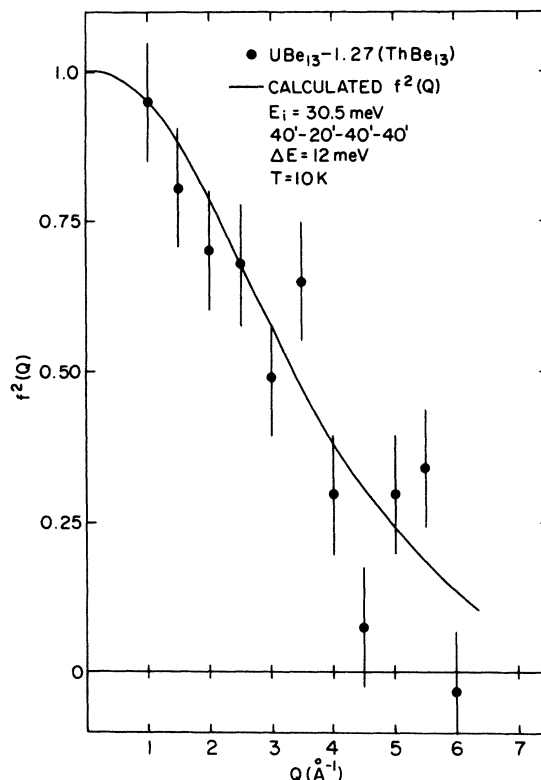


FIG. 3.  $Q$  scan of the difference spectrum at constant energy transfer ( $\Delta E=12 \text{ meV}$ ). The solid line represents the  $\text{U-}5f$  form factor.

confirms the similarity, at least at this energy, of the  $\text{UBe}_{13}$  and  $\text{ThBe}_{13}$  phonon density of states.

Using the integrated intensities of several  $\text{UBe}_{13}$  Bragg powder peaks, and the theoretical cross sections for paramagnetic and nuclear scattering, the difference between the  $\text{UBe}_{13}$  and  $\text{ThBe}_{13}$  spectra in Fig. 2 can be converted to absolute units of  $\mu_B^2/(\text{meV sr})$ , as shown in Fig. 2(b) (see Appendix). This allows a direct comparison of our unpolarized-beam and polarized-beam data, with the bulk susceptibility.

The polarized-beam measurement on  $\text{UBe}_{13}$  taken at  $Q=2.0 \text{ \AA}^{-1}$  is displayed in Fig. 4. An energy scan of the nuclear incoherent scattering, shown in Fig. 4(a) was used to determine the energy resolution of the spectrometer. The magnetic scattering spectrum is shown in Fig. 4(b). Although the energy resolution is coarser and the statistics are clearly poorer than the unpolarized-beam measurements, after converting the magnetic scattering intensity to absolute units, the broad response is in good agreement with the data shown in Fig. 2(b). This provides an important consistency check of our unpolarized measurement subtraction technique. If no reliable nonmagnetic structural analogue of the magnetic compound exists, polarized-beam measurements provide the only unambiguous means to isolate the magnetic scattering contribution. It should also be mentioned that the multiple-scattering contribution to the unpolarized measurements while reduced, may not be totally eliminated. In the polarized-

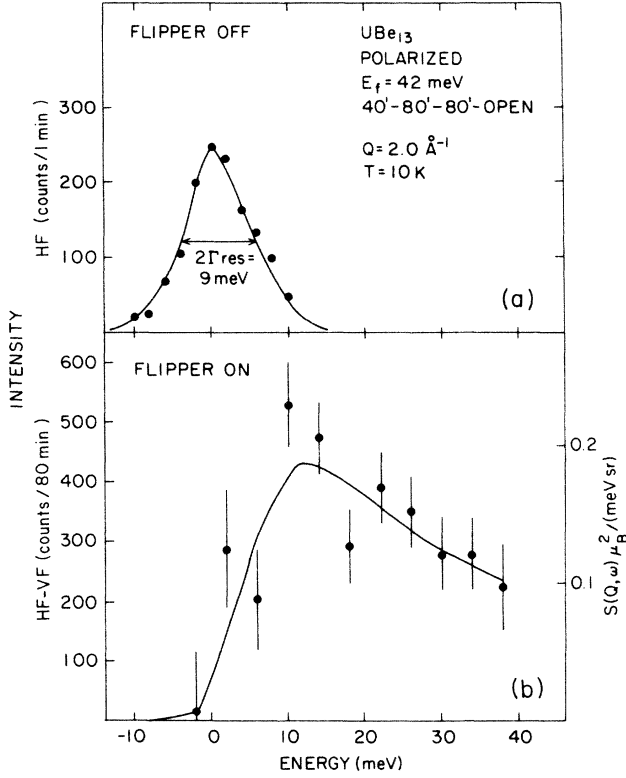


FIG. 4. (a) Constant- $Q$  scan (HF, Flipper off) at  $Q = 2.0 \text{ \AA}^{-1}$  showing the energy resolution of the spectrometer in this configuration. (b) Polarized neutron scattering spectrum of  $\text{UBe}_{13}$  at 10 K. The scale on the left-hand side is the measured intensity, while the scale on the right-hand side is in absolute units. The solid line is the fit to the unpolarized difference spectrum of Fig. 2.

beam measurement, this multiple-scattering contribution is much smaller.

For a cubic paramagnet, the scattering cross section may be written as<sup>9</sup>

$$\frac{d^2\sigma}{d\Omega d\omega} = \gamma_0^2 \frac{k_f}{k_i} \left| \frac{g_j}{2} f(Q) \right|^2 2S^{xx}(Q, \omega) e^{-2W(Q)}, \quad (2)$$

where  $S^{xx}(Q, \omega) = S^{yy}(Q, \omega) = S^{zz}(Q, \omega)$ . In the above,  $\gamma_0^2 = 0.291 \text{ b}$ ,  $f(Q)$  is the magnetic form factor,  $g$  is the Landé  $g$  factor, and  $e^{-2W(Q)}$  is the Debye-Waller factor which, at small  $Q$  and low temperature, is taken as unity. The dynamical structure factor  $S^{xx}(Q, \omega)$ , is the Fourier transform of the magnetic correlations in the system

$$S^{xx}(Q, \omega) = \frac{1}{2\pi} \int dt \sum_r e^{i(Q \cdot r - \omega t)} \langle S_0^x(0) S_r^x(t) \rangle, \quad (3)$$

and can be related to the imaginary part of the susceptibility through the fluctuation-dissipation theorem

$$S^{xx}(Q, \omega) = \frac{1}{\pi} \frac{1}{g^2 \mu_B^2} [n(\omega) + 1] \text{Im}\chi^{xx}(Q, \omega), \quad (4)$$

where

$$[n(\omega) + 1] = (1 - e^{-\omega/kT})^{-1}.$$

In turn,  $\text{Im}\chi^{xx}(Q, \omega)$  may be expressed in terms of the static susceptibility,  $\text{Re}\chi(0)$ , and a spectral weight function,  $P(Q, \omega)$ ,

$$\text{Im}\chi^{xx}(Q, \omega) = \text{Re}[\chi(0)] P(Q, \omega) \omega \pi, \quad (5)$$

where

$$\text{Re}\chi(0) = \frac{g_j^2 J(J+1) \mu_B^2}{3kT} = \frac{M^2 \mu_B^2}{3kT},$$

$$\int_{-\infty}^{\infty} P(Q, \omega) d\omega = 1.$$

$M$  is defined as the effective moment of the system. If all of the  $Q$  dependence is well described by the magnetic form factor,  $P(Q, \omega) \rightarrow P(\omega)$ . For purely relaxational dynamics,

$$P(\omega) = \frac{1}{\pi} \frac{\Gamma}{\Gamma^2 + \omega^2}, \quad (6)$$

where the half-width at half maximum,  $\Gamma$ , is a measure of the magnetization fluctuation energy of the system. At low temperatures ( $kT \ll \Gamma$ ),  $n(\omega) \approx 0$  in Eq. (4), and one directly measures  $\text{Im}\chi(\omega)$  which peaks at  $\omega = \Gamma$ . As temperature increases, and for a temperature-independent  $\Gamma$ , the scattering becomes more symmetric about  $\omega = 0$ .

The magnetic spectra obtained from the polarized- and unpolarized-beam measurements at 10 K were fit using Eqs. (5) and (6) varying  $\Gamma$  and  $\text{Re}\chi(0)$ . These fits are shown in Figs. 2(b) and 4(b). A value of  $13 \pm 2 \text{ meV}$  was obtained for  $\Gamma$ . This energy is much larger than the characteristic energy scale associated with the width of the  $f$ -level resonance implied by the large linear term in the specific heat.<sup>1</sup>

The data in Figs. 2 and 4 are in absolute units and can be compared with the bulk susceptibility as described in the Appendix. For this low-temperature measurement, the real part of the susceptibility may be derived from integrating Eq. (5) through a Kramers-Kronig relation:

$$\text{Re}\chi(0) = \frac{1}{\pi} \int_{-\infty}^{\infty} \frac{\text{Im}\chi(\omega)}{\omega} d\omega. \quad (7)$$

At  $T = 10 \text{ K}$ , using  $\text{Re}\chi_{\text{bulk}} = 12 \times 10^{-3} \text{ emu/mole}^1$ , we obtain

$$\frac{\text{Re}\chi_{\text{neutron}}}{\text{Re}\chi_{\text{bulk}}} = 0.7 \pm 0.2$$

from our polarized and unpolarized neutron scattering measurements. One might expect  $\text{Re}\chi_{\text{neutron}}$  to be somewhat smaller than  $\text{Re}\chi_{\text{bulk}}$  since our integration is limited by the data range and, as seen in Figs. 2 and 4, the magnetic scattering extends out to higher energy. However, since the integration is weighted by  $\omega^{-1}$ , the contribution of this high-energy region is small. Thus, within error, the magnetic susceptibility is nearly exhausted by the broad scattering we have measured. Any additional response must have a small spectral weight.

Unpolarized-beam measurements with higher-energy resolution were performed in order to search for a narrow quasielastic feature in the spectrum. Figure 5 shows data taken at  $Q = 0.4 \text{ \AA}^{-1}$  with a fixed initial energy of 5.0 meV at 0.35 and 4.2 K using a  $^3\text{He}$  cryostat. No difference between the two temperatures is observed, whereas a

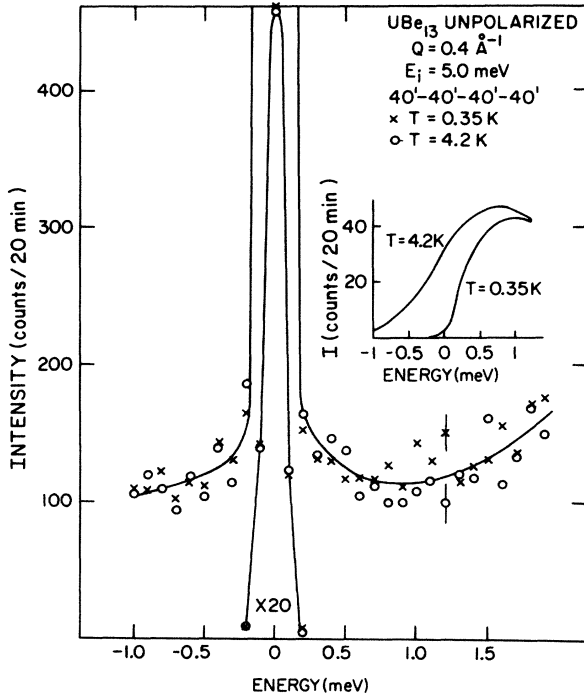


FIG. 5. High-resolution, constant- $Q=0.4 \text{ \AA}^{-1}$  scan of the small energy-transfer region of the unpolarized neutron scattering spectrum of  $\text{UBe}_{13}$  at  $T=0.35$  and  $4.2 \text{ K}$ . Inset: Calculated magnetic contribution to the inelastic spectrum assuming a quasielastic feature with  $\Gamma=1 \text{ meV}$  and a spectral weight of  $1\mu_B$ .

narrow quasielastic feature which carries significant spectral weight, would be evidenced by greater scattered intensity on the energy gain side at the higher temperature. This is illustrated in the inset of Fig. 5, which shows the calculated magnetic scattering contribution to the inelastic spectrum at the two temperatures for a quasielastic half-width,  $\Gamma=1 \text{ meV}$  and spectral weight appropriate to  $M^2=1\mu_B^2$ .

The data shown in Fig. 5 were taken above and below the superconducting transition temperature for  $\text{UBe}_{13}$  ( $T_c \approx 0.9 \text{ K}$ ). At the higher temperature, it is expected that additional scattering should be observed for energy transfer smaller than the gap energy [ $E_g(0) \approx 3.53k_B T_c$ ], which is about  $0.3 \text{ meV}$ . Again, no difference in scattering between the two temperatures is observed.

#### IV. DISCUSSION

It remains a puzzle why the neutron measurements, which directly couple to the response of the  $f$  electrons, do not exhibit the narrow, quasielastic response expected on the basis of the specific-heat measurements. The meaning of the broad response is not totally clear. However, it is interesting to note that the energy scale we obtain,  $\Gamma \approx 13 \text{ meV}$ , is close to the temperature range where the bulk susceptibility deviates from a Curie-Weiss

behavior. The high-temperature Curie-Weiss behavior of this system might normally be expected to result in magnetic ordering at lower temperatures. Some mechanism,<sup>1</sup> perhaps the Kondo effect or valence fluctuations between equivalent  $f$ -electron magnetic and nonmagnetic ground states seems to interfere with the formation of magnetic long-range order.

The spectra of Figs. 2 and 4 bear a striking resemblance to the mixed valent materials. In fact, measurements on the isostructural mixed valent compound  $\text{CeBe}_{13}$  (Ref. 7) also exhibit a broad magnetic response with  $\Gamma \approx 25 \text{ meV}$ . This can be contrasted with magnetic neutron scattering measurements on  $\text{CeCu}_2\text{Si}_2$  by Horn *et al.*,<sup>3</sup> where the half-width,  $\Gamma$ , of the quasielastic line was found to be  $\approx 1 \text{ meV}$ . It was concluded in this study that the spin-relaxation behavior of the Ce  $4f$  electrons is dominated by Kondo-type spin fluctuations. The half-width of the quasielastic scattering for  $\text{CeCu}_2\text{Si}_2$  seems to scale in some manner with the specific-heat measurements. In addition, as the temperature is lowered, the measured bulk susceptibility of  $\text{CeCu}_2\text{Si}_2$  deviates to a larger value, while the deviation measured in  $\text{UBe}_{13}$  tends to a smaller value.<sup>1</sup> This difference in behavior, as well as the neutron scattering results for  $\text{UBe}_{13}$ , indicates that the mechanism which suppresses magnetic ordering in  $\text{UBe}_{13}$  may be different from that responsible in this other heavy-fermion system.

Recently, Overhauser and Appel<sup>12</sup> have proposed an  $s$ - $f$  hybridization model which predicts a low-frequency Einstein mode in  $\text{UBe}_{13}$  in order to account for the proposed large lattice contribution to the specific heat at low temperatures. This mode is associated with the U atoms in  $\text{UBe}_{13}$ , and must be lower than the corresponding mode associated with the Th atoms in  $\text{ThBe}_{13}$ . Our measurements indicate that the phonon density of states for  $\text{UBe}_{13}$  and  $\text{ThBe}_{13}$  are closely similar. The difference in scattering between these two materials was demonstrated to be of purely magnetic origin. If the feature at  $\omega=13 \text{ meV}$  in Fig. 2 is identified as this low-lying mode, its observation in both  $\text{ThBe}_{13}$  and  $\text{UBe}_{13}$  is inconsistent with the model of Overhauser and Appel, and no other sharp feature in the  $\text{UBe}_{13}$  spectrum was identified down to  $\omega=0.5 \text{ meV}$ .

In conclusion, we have observed a broad ( $\Gamma \approx 13 \text{ meV}$ ) quasielastic response in the magnetic scattering spectrum of polycrystalline  $\text{UBe}_{13}$  which is inconsistent with the narrow resonance predicted from specific-heat measurements. Within experimental error, the susceptibility calculated from the energy integrated magnetic scattering is consistent with bulk measurements. In addition, no difference in the susceptibility is observed above and below the superconducting transition. Further studies of the temperature dependence of the inelastic magnetic spectrum of  $\text{UBe}_{13}$  are currently underway.

#### ACKNOWLEDGMENTS

We thank G. Aeppli, J. D. Axe, B. Battlog, P. Böni, J. Martinez, J. Wicksted, K. Tajima, C. Stassis, C. M. Varma, Y. J. Uemura, and H. Yoshizawa for extensive discussions. The work at Brookhaven National Laboratory was supported by the Division of Materials Sciences, U.S. Department of Energy under Contract No. DE-AC02-

76CH00016, and at Los Alamos National Laboratory by the U.S. Department of Energy.

### APPENDIX

In this appendix we show how the measured paramagnetic scattering data can be converted to absolute units for comparison with bulk-susceptibility measurements. Previous workers<sup>8</sup> have described this procedure for the case of a single crystal using the measured and theoretical cross sections for phonons. For polycrystalline material, Ziebeck and Brown<sup>13</sup> have used Bragg powder peaks to calculate an absolute intensity scale for their magnetic scattering data. In their procedure however, the calibration was performed by measuring the paramagnetic scattering at a single point, with the spectrometer set for zero-energy transfer and the assumption that the energy resolution of the spectrometer allows the proper energy integration of the paramagnetic scattering. Although this is reasonable for the case where the half-width of the paramagnetic spectrum,  $\Gamma$ , is much smaller than the resolution of the spectrometer,  $\Gamma_{\text{res}}$ , significant contributions to the susceptibility can be missed if  $\Gamma > \Gamma_{\text{res}}$ . For this case, energy scans through the paramagnetic spectrum must be performed, and the method described by Ziebeck *et al.*<sup>13</sup> must be suitably modified. Böni *et al.*<sup>14</sup> have performed such energy scans, and the conversion to an absolute basis is accomplished by assuming a reasonable spectral weight function, and then integrating this function. Here we describe a procedure which does not rely upon a model for the scattering function, but rather converts the raw data itself to absolute units.

The energy integrated paramagnetic scattering per monitor count measured in an energy scan at constant  $Q$  may be written as

$$J_{\text{pm}} = \Delta\omega \sum_{\omega \in (\omega_i, \omega_f)} I_{\text{pm}}(\omega) = \Delta\omega \sum_{\omega \in (\omega_i, \omega_f)} \frac{d^2\sigma\omega}{d\Omega d\omega} \frac{N_m V}{V_c}, \quad (\text{A1})$$

where the indices  $i$  and  $f$  denote the initial and final states of the measurement.  $I_{\text{pm}}$  is the magnetic scattering intensity measured at each step,  $\Delta\omega$ , in the unpolarized-beam measurement or twice (HF-VF) measured in a polarized-beam experiment.  $N_m$ ,  $V$ , and  $V_c$  are the number of magnetic atoms per unit cell, the volume of the sample, and the unit-cell volume, respectively. In order to put  $J_{\text{pm}}$  on an absolute scale, the integrated intensity per monitor count of a Bragg powder peak is used. Therefore,

$$J_{\text{Bragg}} = \left[ \Delta(2\theta) \sum_{2\theta \in (2\theta_i, 2\theta_f)} I_{\text{Bragg}}(2\theta) \right] (2\Gamma_{\text{res}}). \quad (\text{A2})$$

Here,  $I_{\text{Bragg}}$  is the intensity measured in an elastic scan around a Bragg peak taken in steps of  $\Delta 2\theta$  (radians).  $\Gamma_{\text{res}}$  is the half-width at half maximum of the energy resolution, and may be measured by an energy scan of the incoherent scattering.

The integrated paramagnetic scattering in units of  $\mu_B^2$  is then calculated from

$$M^2 = C \frac{J_{\text{pm}}}{J_{\text{Bragg}}}, \quad (\text{A3})$$

$$C = \frac{1}{0.0485 [f(Q)]^2} \frac{1}{8\pi} \frac{\lambda^3 P F^2}{N_m V_c \sin\theta \sin(2\theta)},$$

where  $F$  and  $P$  are the structure factor for the powder reflection and its multiplicity, respectively. The constant 0.0485 is  $\lambda_0^2/6$ , where  $\lambda_0 = 0.291$  b.

$\text{Re}\chi(0)$  may be calculated from the measured magnetic scattering intensity by

$$\text{Re}\chi(0) = \frac{1}{\pi} \int \frac{\text{Im}\chi(Q, \omega)}{\omega} d\omega$$

$$\approx \Delta\omega \sum_{\omega \in (\omega_i, \omega_f)} \frac{I_{\text{pm}}(\omega)}{\langle n(\omega) + 1 \rangle} \frac{1}{\omega} \frac{C}{J_{\text{Bragg}}}. \quad (\text{A4})$$

At high temperatures where  $kT \gg \Gamma$ ,  $\langle n(\omega) + 1 \rangle \approx kT/\omega$ , and using Eqs. (A1) and (A3) (Ref. 15)

$$\text{Re}\chi(0) = 0.125 M^2 (\mu_B^2) / T (\text{K}) \text{ emu/mole}. \quad (\text{A5})$$

This expression is just Curie's law for an ideal paramagnet. For systems with strong magnetic correlations, the denominator in Eq. (A5) takes the Curie-Weiss form,  $T + \Theta$ . At low temperatures  $\text{Re}\chi(0)$  must be calculated directly from Eq. (A4).

We now illustrate the procedure outlined above through a calculation of  $M^2$  and  $\text{Re}\chi(0)$  for  $\text{MnF}_2$  at room temperature. The paramagnetic scattering from  $\text{MnF}_2$  was measured by polarized neutrons using spectrometer configuration (e) in Table II. The data shown in Fig. 6 represents the difference (HF-VF) at  $|Q| = 1.0 \text{ \AA}^{-1}$ , and yields  $\frac{1}{2}$  of the unpolarized-beam magnetic cross section. Therefore,  $I_{\text{pm}}$  must be multiplied by a factor of 2. Using the known structure of  $\text{MnF}_2$  (Ref. 16) and the (101) powder reflection, we obtain

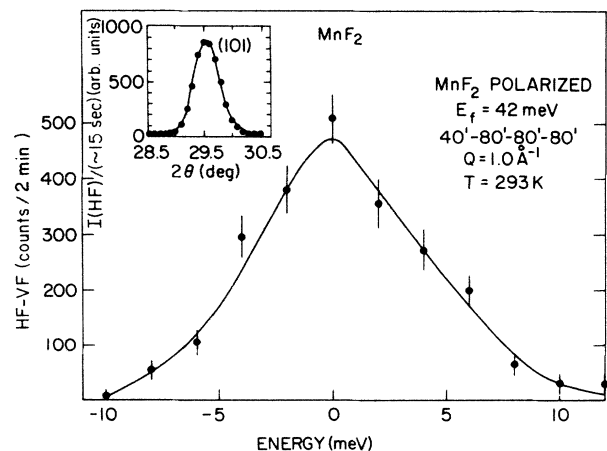


FIG. 6. Constant- $Q$  scan (HF-VF) for  $\text{MnF}_2$  at  $T = 293$  K. Inset: Elastic scan of the  $\text{MnF}_2$  (101) Bragg powder peak at  $T = 293$  K.

$$J_{\text{pm}} = (2 \times 2 \text{ meV/step})(2300/2 \text{ min})$$

$$= 9200 \text{ counts meV/2 min ,}$$

$$J_{\text{Bragg}} = 710 \text{ counts meV/2 min .}$$

$$\Delta\omega = 2 \text{ meV; } \Delta 2\theta = 1.75 \times 10^{-3} \text{ rad; } 2\Gamma_{\text{res}} = 8 \text{ meV;}$$

$$C = 2.6 ,$$

$$M^2 = 2.6 \times \frac{9200}{710} = 33.7 \mu_B^2; M = 5.8 \mu_B .$$

We note that our measured value of  $M$  is only 3% smaller than the known effective moment of  $\text{Mn}^{2+}$  ( $M = 5.95 \mu_B$ ). We can also calculate  $\chi(0)$  from Eq. (A.5) as

$$\begin{aligned} \chi(0) &= 0.125085 \frac{M^2}{T + \Theta} \text{ emu/mole} \\ &= 10.8 \times 10^{-3} \text{ emu/mole ,} \end{aligned}$$

for  $\Theta = 97 \text{ K}$ . This compares well with the bulk value, obtained by Corliss *et al.*,<sup>17</sup> of  $11.5 \times 10^{-3} \text{ emu/mole}$ .

<sup>1</sup>G. R. Stewart, *Rev. Mod. Phys.* **56**, 755 (1984).

<sup>2</sup>H. R. Ott, H. Rudigier, Z. Fisk, and J. L. Smith, *Phys. Rev. Lett.* **50**, 1595 (1983).

<sup>3</sup>S. Horn, E. Holland-Moritz, M. Loewenhaupt, F. Steglich, H. Scheuer, A. Benoit, and J. Flouquet, *Phys. Rev. B* **23**, 3171 (1981).

<sup>4</sup>G. Aeppli, E. Bucher, and G. Shirane, *Phys. Rev. B* **32**, 7579 (1985).

<sup>5</sup>H. C. Baenziger and R. E. Rundle, *Acta Cryst.* **2**, 258 (1949).

<sup>6</sup>A. I. Goldman, S. M. Shapiro, D. E. Cox, J. L. Smith, and Z. Fisk, *Phys. Rev. B* **32**, 6402 (1985).

<sup>7</sup>E. Holland-Moritz, D. Wohlleben, and M. Loewenhaupt, *Phys. Rev. B* **25**, 7482 (1982).

<sup>8</sup>O. Steinsvoll, C. F. Majkrzak, G. Shirane, and J. P. Wicksted, *Phys. Rev. B* **30**, 2377 (1984); J. P. Wicksted, P. Böni, and G. Shirane, *ibid* **30**, 3655 (1984).

<sup>9</sup>W. Marshall and S. W. Lovesey, *Theory of Thermal Neutron Scattering* (Clarendon, Oxford, 1971).

<sup>10</sup>Here the normalization factor of 1.27 results from a slightly different UBe<sub>13</sub> sample volume in this measurement.

<sup>11</sup>B. C. Frazer, G. Shirane, D. E. Cox, and C. E. Olsen, *Phys. Rev.* **140**, 1448 (1965); J. Faber, Jr. and G. H. Lander, *Phys. Rev. B* **14**, 1151 (1975).

<sup>12</sup>A. W. Overhauser and J. Appel, *Phys. Rev. B* **31**, 193 (1985).

<sup>13</sup>K. R. A. Ziebeck and P. J. Brown, *J. Phys. F* **10**, 2015 (1980).

<sup>14</sup>P. Böni, G. Shirane, J. P. Wicksted, and C. Stassis, *Phys. Rev. B* **31**, 4597 (1985).

<sup>15</sup>Y. J. Uemura (private communication).

<sup>16</sup>R. W. G. Wyckoff, *Crystal Structures* (Interscience, New York, 1963), Vol. 1, p. 251.

<sup>17</sup>L. Corliss, Y. Delabarre, and N. Elliot, *J. Chem. Phys.* **18**, 1256 (1950).